minerals

MDPI

Article

Mineralogical Characteristics and Leaching Behavior of Sandstone-Hosted Uranium Ore: Implications for In Situ Recovery in the Zhenyuan Deposit, SW Ordos Basin, China

Chunru Hou [1,*], Shihai Chen [2], Ying Zhang [2], Zhengbang Liu [1], Xiansheng Xie [3], Jinxun Deng [1], Yuhan Zou [1] and Wensheng Liao [1]

[1] Beijing Research Institute of Chemical Engineering and Metallurgy, CNNC, Beijing 101149, China; liuzb@cnmstc.com (Z.L.); dengjinxun@cnmstc.com (J.D.); zyh@cnmstc.com (Y.Z.); liaows@cnmstc.com (W.L.)
[2] PetroChina Changqing Oilfield Company, Xi'an 710018, China; 17702969088@163.com (S.C.); a235947087@163.com (Y.Z.)
[3] China Shaanxi Nuclear Industry Group Geological Survey Institute Co., Ltd., Xi'an 710100, China; 18586476742@163.com
* Correspondence: chunruhou@cnmstc.com

Abstract

The mineralogical composition, textural characteristics, and uranium occurrence of sandstone-hosted uranium ores significantly influence the leaching performance during in situ recovery. This study investigates ore samples from the Zhenyuan uranium deposit, China, utilizing SEM, EPMA, XRD, and XRF to characterize their texture and mineralogy. Combined with thin-section leaching tests, batch stirring experiments, and pressurized column leaching experiments, the leaching behavior of pitchblende, associated gangue minerals, and the whole rocks were evaluated. The results indicate that: Uranium mainly occurs as nano-spherical and film-like pitchblende distributed along the edges of detrital grains and Ti-oxides. Minor uranium is incorporated into Ti-oxides and dolomite lattices via isomorphic substitution or adsorbed by chlorite. Under CO_2 + O_2 leaching conditions, pitchblende was almost completely dissolved, while U-bearing Ti-oxides experienced slight corrosion. Dolomite underwent partial dissolution, providing bicarbonate ions and improving rock permeability. Pyrite dissolution was limited during the early stage of leaching. The high dolomite content, low clay abundance, favorable pore structure, and easily leachable pitchblende suggest that the Zhenyuan deposit is well suited for CO_2 + O_2 in situ recovery. Increasing CO_2 pressure is recommended to enhance dolomite dissolution and improve uranium recovery efficiency.

Keywords: sandstone-hosted uranium deposit; pitchblende; leaching; CO_2 + O_2; Zhenyuan uranium deposit

Academic Editor: Ilhwan Park

Received: 24 February 2026
Revised: 14 March 2026
Accepted: 19 March 2026
Published: 24 March 2026

1. Introduction

With increasing global demand for clean and stable energy, nuclear power continues to play a vital role in energy transition strategies. Uranium, as the primary fuel for nuclear power generation, has become strategically important. Sandstone-hosted uranium deposits represent the most important uranium resource type in China and are predominantly exploited using in situ recovery (ISR) technology [1].

In ISR, groundwater is first pumped to the surface via extraction wells. Leaching reagents are then added to the groundwater, which is injected back into the ore-bearing

aquifer through injection wells, dissolving uranium minerals and mobilizing uranium from the solid phase into the groundwater. The uranium-bearing groundwater is subsequently extracted to the surface and uranium is subsequently recovered at the surface using ion-exchange resins [1].

ISR uranium extraction is classified by the type of chemical reagent added: Acid leaching (sulfuric acid), alkaline leaching (sodium bicarbonate + ammonium bicarbonate), and CO_2 + O_2 leaching [1]. Since ISR minimally alters the ore's original texture and mineral composition, ISR performance is strongly controlled by the mineralogical composition, textural features, and uranium occurrence of the ores [2–7]. Uranium minerals are typically the primary hosts of uranium in deposits [8], but different uranium minerals exhibit different dissolution kinetics under varying lixiviant systems, including acidic, alkaline, and CO_2 + O_2 systems [9–11]. Even the same uranium mineral may display different leaching behaviors depending on impurity content and crystal chemistry [12,13]. Generally, uranium minerals leach faster and more completely under acid conditions compared to other reagents. Beyond uranium mineral types, their contact relationships with other minerals and degree of liberation also affect leaching [14,15]. For instance, highly liberated uranium minerals have a greater contact area with leaching agents, facilitating extraction. Uranium minerals encapsulated by insoluble silicates like feldspar-quartz are difficult to access and leach. Those encapsulated by soluble minerals like calcite require higher CO_2 concentrations to dissolve the calcite and increase uranium liberation. Additionally, other gangue minerals in the ore can significantly influence leaching process selection. Carbonate minerals significantly influence leaching chemistry. In acid systems, their dissolution increases acid consumption and may lead to $CaSO_4$ precipitation, causing pore clogging and permeability reduction [7,16–18]. In contrast, under CO_2 + O_2 conditions, carbonate dissolution provides bicarbonate ligands necessary for uranyl complexation [13]. Sulfide minerals such as pyrite may consume oxygen and produce $Fe(OH)_3$ precipitates, potentially impairing permeability [4,13,19–21]. Therefore, detailed mineralogical characterization is essential for optimizing ISR strategies.

This study focuses on the Zhenyuan sandstone-hosted uranium deposit in the southwestern Ordos Basin. By integrating mineralogical analysis with laboratory leaching experiments, we evaluate uranium occurrence, the dissolution behavior of uranium and gangue minerals, and identify the most suitable leaching process.

2. Geological Setting

The Zhenyuan uranium deposit is located in the southwestern Ordos Basin and hosted in the Lower Cretaceous Huanhe Formation (Figures 1 and 2). The Huanhe Formation conformably contacts the overlying Luohandong Formation and underlying Luohe Formation. Based on lithological assemblages, the Huanhe Formation is divided into upper and lower members. The upper member consists mainly of thick mudstone and siltstone, while the lower member features medium- to fine-grained sandstone interbedded with thin siltstone and mudstone. The ore bodies mainly occur within the lower member of the formation along oxidation–reduction transition zones. Orebody is approximately 4.5 km wide (north–south). It is hosted in gray to light-yellow sandstones at depths ranging from 681 to 932 m, with an average thickness of 15.95 m and an average grade of 0.0261% U.

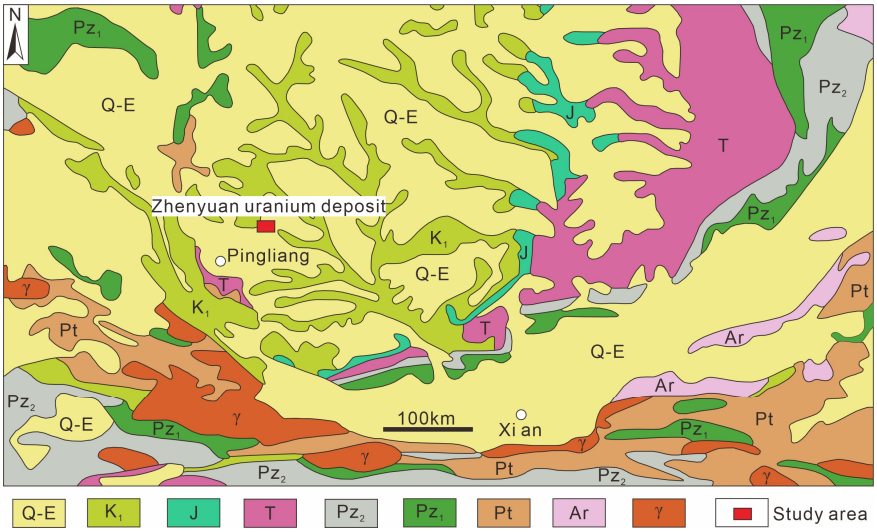

Figure 1. Geological map of Zhenyuan sandstone-hosted uranium deposit [17]. Q-E: Neogene to Quaternary; K_1: Upper Cretaceous; J: Jurassic; T: Triassic; Pz_2: Upper Paleozoic; Pz_1: Lower Paleozoic; Pt: Proterozoic; Ar: Archean.

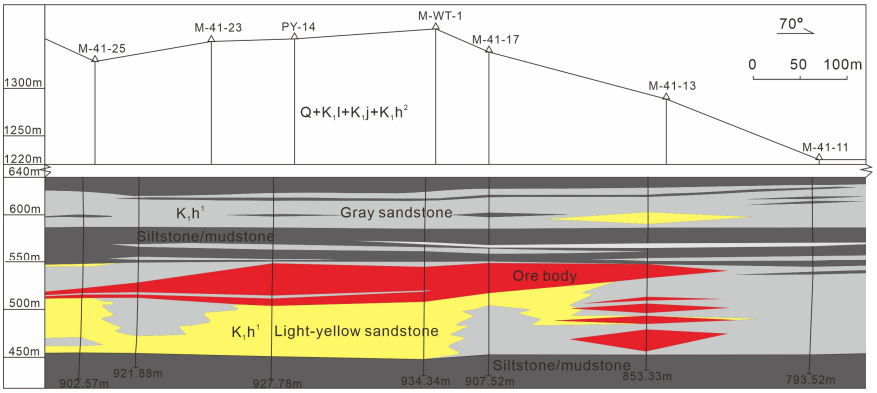

Figure 2. Geological cross-section of Zhenyuan sandstone-hosted uranium ore body [17].

3. Materials and Methods

Thirty core samples from five drills were collected for mineralogical investigation and leaching experiments. Thin sections were prepared for SEM observation and in-suit leaching tests. SEM analysis was conducted using a ThermoFisher (Waltham, MA, USA) Nova Nano SEM450 at the Beijing Research Institute of Uranium Geology, with an accelerating voltage of 15 kV and working distance of 5–10 mm. XRD analysis was performed using a Bruker (Billerica, MA, USA) Panalytical X'Pert PRO X-Ray diffractometer at the Beijing Research Institute of Uranium Geology, with operating conditions of 40 kV and 40 mA, and a scanning range of 5–70°. EPMA analyses were performed on JEOL (Tokyo, Japan) JXA-IHP200F at the Beijing Research Institute of Uranium Geology, with an accelerating voltage of 15 kV, working current of 10^{-8} A, working distance of 5–10 mm.

Thin-section leaching test: Thin-section leaching was conducted under conditions of 0.2 MPa CO_2 + 1 MPa O_2. The process involved introducing 0.2 MPa CO_2 for 4 h, followed by 1 MPa O_2 for 7 days at room temperature. Before leaching, the morphology of pitchblende and gangue minerals was observed, and their locations were documented using SEM. After leaching, the pre-observed uranium and gangue minerals were relocated for morphological comparison.

Acid Stirring Leaching: Each experiment used 60 g of ore sample mixed with 300 mL of sulfuric acid solution prepared with groundwater in ore-bearing aquifer, stirred for 24 h at room temperature.

Alkaline Stirring Leaching: Each experiment used 60 g of ore sample mixed with 300 mL of NH_4HCO_3 solution prepared with ore-bearing aquifer water, stirred for 72 h at room temperature.

CO_2 + O_2 Pressurized Stirring Leaching: Each experiment used 60 g of ore sample with 300 mL of ore-bearing aquifer water. During the experiment, 0.2 MPa CO_2 was introduced for 3 h every 48 h, while O_2 was introduced for the remaining time until the end.

CO_2 + O_2 Pressurized Column Leaching Test: The column leaching test was conducted under the following conditions: 700 g of ore sample was packed into a stainless-steel column with an inner diameter of 25 mm, resulting in a packing height of approximately 1000 mm, a packed volume of 491 mL, and a packing density of 1.43 kg/L. After packing, a certain volume of ore-bearing aquifer water was first passed through the column to pre-wet the ore bed. The effluent from this pre-wetting stage was collected and analyzed. A cumulative volume of 1200 mL of ore-bearing aquifer water effluent was obtained, with a uranium concentration of 14 mg/L. This corresponded to the leaching of 0.0168 g of metallic uranium, yielding an initial recovery of 7.74%. Subsequently, the formal CO_2 + O_2 pressurized leaching commenced by injecting a leaching agent prepared by saturating ore-bearing aquifer water with carbon dioxide and oxygen. The gas pressures were set at 0.2 MPa for CO_2 and 1.0 MPa for O_2. The effluent flow rate was controlled to simulate the hydrodynamic conditions of an underground in situ leaching operation. The effluent volume and uranium concentration were recorded daily. The leaching process continued until the uranium concentration in the effluent consistently fell below 3 mg/L, which lasted for a total of 68 days from the start of lixiviant injection. The final liquid (mL)-to-solid (mg) (L/S) ratio reached 5.18, and the cumulative leaching recovery was 68.45%.

4. Results

4.1. Mineralogical and Chemical Composition

Whole-rock and clay XRD analyses indicate that the mineral composition of sandstone samples from the Zhenyuan deposit is relatively consistent, primarily consisting of quartz (average 86.36 wt%), plagioclase (average 4.53 wt%), K-feldspar (average 2.72 wt%), dolomite (average 5.45 wt%) (Table 1). Clay minerals are mainly illite (average 85 wt%), kaolinite, and minor chlorite. Calcite content varies between 0 wt% and 5.3 wt%, present only in a few ore samples. Clay mineral content varies between 0.3 wt% and 4.4 wt% (average 1.68 wt%).

The chemical composition of ore from the lower Huanhe Formation is essentially similar to that of the surrounding rock, dominated by Si, Al, Ca, K, Mg, and Fe. SiO_2 content is high, with average values of 83.97% in ore and 84.25% in wall rock, consistent with the high quartz content. Average Al_2O_3 content is 4.95% in ore and 5.06% in wall rock. The average content of the sensitive element CaO during ISR is 2.36% in ore and 2.13% in wall rock. Average MgO content is 1.16% and 1.11%, respectively. Average Fe_2O_3 content is 1.17% in both.

4.2. Ore Texture

The ore is primarily light gray to gray, fine- to medium-grained feldspathic lithic sandstone and medium- to fine-grained feldspathic quartz sandstone. The ore is mainly composed of quartz, dolomite, plagioclase, K-feldspar, and clay minerals (Table 1), along with heavy minerals such as rutile, anatase, pyrite, and zircon. The ore exhibits an inequigranular sandy texture, with moderate to good sorting and subangular to subrounded roundness, primarily in a grain-supported framework with point contacts (Figure 3A,B). Cement is mainly dolomite, followed by minor sericite, chlorite, biotite, and iron oxides, distributed along intergranular spaces and edges of quartz and feldspar clasts (Figure 3C–F).

Table 1. XRD results of ore samples in Zhenyuan uranium deposit (wt%).

Sample Number	Quartz	K-Feldspar	Plagioclase	Calcite	Dolomite	Clay
M-WT-5-KY-001	80.6	4.7	6.7	/	6.5	1.5
M-WT-5-KY-005	84.0	2.9	5.8	/	6.1	1.1
M-WT-5-KY-006	79.1	4.9	4.7	/	8.2	3.1
M-WT-5-KY-007	82.1	3.2	4.6	/	8.0	2.2
M-WT-5-KY-010	88.0	1.9	3.0	/	5.9	1.3
M-WT-5-KY-012	88.7	1.7	2.4	/	5.7	1.5
M-29-31-KY-001	87.6	3.0	3.8	4.0	/	1.5
M-29-31-KY-002	87.4	4.0	7.4	/	/	1.2
M-29-31-KY-003	85.7	3.7	6.3	1.2	1.8	1.3
M-29-31-KY-004	89.0	3.1	6.4	/	/	1.5
M-29-31-KY-005	92.3	2.2	/	5.3	/	0.3
M-29-31-KY-008	85.9	2.3	4.3	/	5.7	1.9
17-15-KY-001	88.9	2.2	2.9	/	4.1	1.9
17-15-KY-002	89.2	0.8	/	/	8.2	1.7
17-15-KY-004	88.3	2.1	2.3	/	6.9	0.3
17-15-KY-005	87.6	2.5	4.3	/	4.9	0.7
17-15-KY-007	92.4	1.3	1.9	/	3.9	0.6
M-47-15B-KY-002	86.1	2.5	3.5	3.7	/	4.1
M-47-15B-KY-004	86.3	2.9	3.3	4.4	2.6	0.4
M-47-15B-KY-008	89.1	1.9	3.1	/	4.3	1.5
M-47-15B-KY-010	92.4	1.8	/	/	4.0	1.8
M-47-15B-KY-013	91.4	1.0	2.4	/	3.0	2.3
M-47-15B-KY-014	86.2	2.6	3.5	/	6.6	1.2
M-47-15B-KY-015	91.7	1.3	3.2	/	2.8	0.9
M-37-21-24(10/12)	80.9	3.6	6.9	/	4.2	4.4
M-37-21-26(6/36)	89.5	2.7	3.3	/	3.1	1.4
M-37-21-27(10/19)	81.7	3.9	7.4	/	6.5	0.4
M-37-21-28(2/28)	79.2	3.3	7.5	/	7.2	2.8
M-37-21-28(7/28)	82.5	3.0	4.6	/	8.0	1.9
M-37-21-30(5/7)	77.1	4.5	6.8	/	8.1	3.6

Feldspar and quartz constitute the sandstone framework (Figure 3A,B). Quartz mostly displays anhedral granular texture with relatively good roundness (subangular to subrounded). Some grains show secondary overgrowths at edges, with particle sizes ranging from 0.2 mm to 0.8 mm. Some grains contain micro-fractures. Pressure solution structures, forming stylolites or pressure-solution embayments, are common at contacts between quartz and other minerals (Figure 3C). Feldspar, primarily plagioclase and K-feldspar, is mostly subangular, with a minor portion being subrounded, and particle sizes ranging from 0.1 mm to 0.5 mm. Feldspar grains often contain micro-fractures. Plagioclase exhibits polysynthetic twinning and alterations such as argillization and sericitization. K-feldspar is mainly microcline, displaying cross-hatched twinning.

Carbonate minerals in the ore are predominantly dolomite and calcite (Table 1). Based on morphology, dolomite can be classified into two types (Figure 3E,F): Euhedral dolomite and anhedral dolomite. Euhedral dolomite particles exhibit rhombohedral structures, approximately 10 μm in size, distributed along the edges of feldspar and quartz clasts or filling pores (Figure 3F). Anhedral dolomite is elliptical, approximately 100–200 μm in size. Calcite particles show euhedral rhombic crystal structures, about 10 μm in size. Dolomite and calcite are independently distributed in the ore, with only a few samples containing both. Clay minerals fill pores in a flaky or vermicular form and are unevenly distributed, often occurring in clusters (Figure 3D).

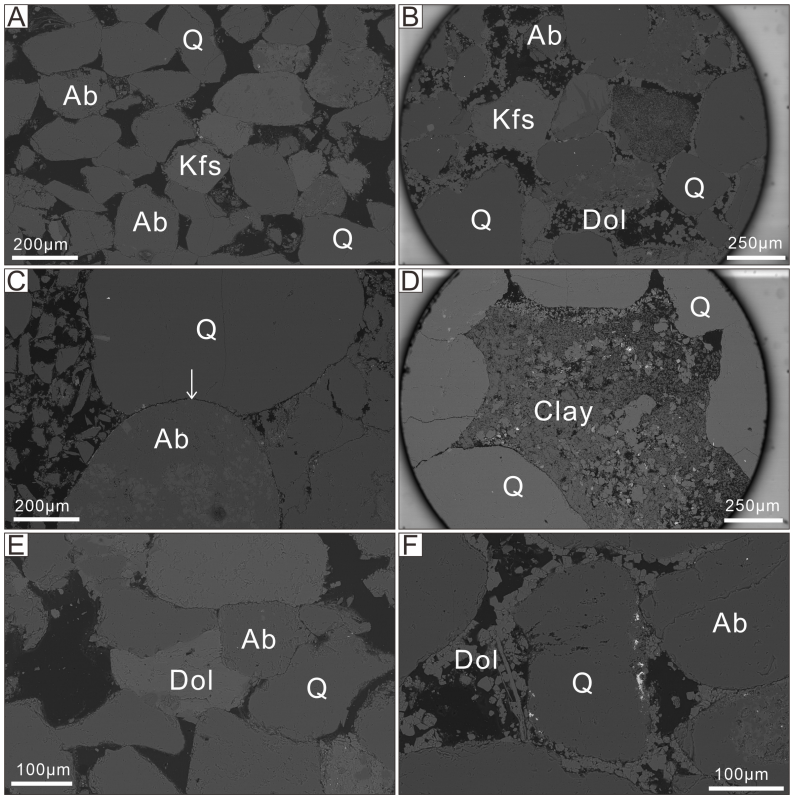

Figure 3. Microstructures of ore samples in Zhenyuan uranium deposit. (**A**) Quartz and feldspar constitute the framework of ore, with detrital grains exhibiting an elliptical shape, grain sizes averaging around 200 μm, and good sorting; (**B**) Dolomite acts as the cementing material, filling the majority of the pore spaces; (**C**) Pressure-solution structures are developed at the contact interfaces between quartz and feldspar (White arrow); (**D**) Clay minerals partially fill the pores within the sandstone; (**E**) Anhedral dolomite displays an interstitial texture, forming the cement; (**F**) Dolomite grains distributed along grain boundaries. Q: Quartz; Ab: Ablite; Kfs: K-feldspar; Dol: Dolomite.

4.3. Porosity and Permeability

Porosity measurements indicate ore porosity ranges between 18% and 29%, with an average of approximately 25% (Table 2). Over 90% of tested samples have porosity exceeding 20%. Gas permeability among samples varies between 67 mD and 2214 mD, with an average of approximately 640 mD. Over 80% of tested samples have gas permeability exceeding 200 mD. Liquid permeability ranges from 206 mD to 873 mD. Both gas and liquid permeability show a positive correlation with sample porosity. However, the variation in permeability is significantly greater than that in porosity, especially among samples with higher porosity, where permeability differences are more pronounced compared to samples with lower porosity.

Table 2. Porosity, liquid permeability, and gas permeability of ore samples.

Sample Number	Porosity (%)	Liquid Permeability (mD)	Gas Permeability (mD)
M-37-21 26(6/36)	29.27	389.22	443.08
M-37-21 20(19/24)	25.18	792.56	1692.04
M-37-21 28(7/28)	26.54	430.28	678.71
M-29-31 KY001	20.35	205.97	202.87
M-29-31 KY002	23.38	589.31	916.00
M-29-31 KY004	27.84	873.43	2214.13

4.4. Uranium Occurrence

SEM and EPMA results show that uranium in the Zhenyuan sandstone uranium deposit primarily exists as pitchblende. Additionally, a minor amount of uranium occurs in isomorphism within Ti-oxides and dolomite. Some uranium is also adsorbed by chlorite.

Pitchblende is primarily composed of uranium, with UO_2 content ranging from 51.89 wt% to 82.15 wt% (average 71.6 wt%). It also contains certain amounts of Ca, Si, Ti, Na, P, S, Al, Pb, Fe, etc. Among these, Ca, Si, and Ti contents exceed 2 wt%, while other elements are generally below 2 wt% (Table 3). Uranium content in pitchblende shows a coordinated variation trend with calcium content, whereas silicon and titanium contents show an inverse relationship with uranium content. Based on morphology, pitchblende can be divided into two categories (Figure 4): One consists of nano-spherical particle aggregates (200–300 nm in diameter), mainly distributed along the edges of feldspar-quartz clasts or surrounding clay and organic matter (Figure 4A,B). Some nano-spherical uranium minerals are closely associated with Ti-oxides, distributed along the edges of euhedral Ti-oxides particles, forming core-mantle structures. Some nano-spherical pitchblende grows around nano-sized Ti-oxide cores (Figure 4D). Pitchblende also occurs as films growing on the edges of Ti-oxides (Figure 4C). Some titanium oxide and pitchblende intergrowths, forming Ti-oxides and pitchblende aggregates (Figure 4E,F).

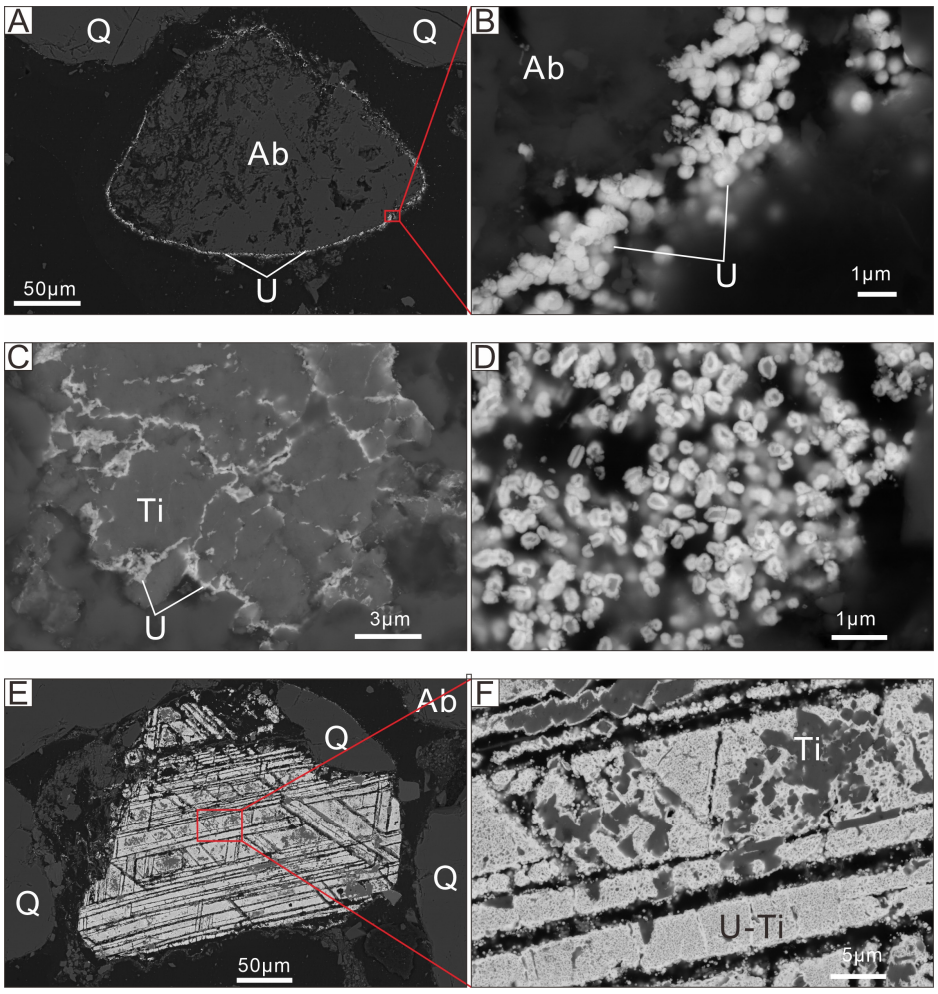

Figure 4. (**A**,**B**) Nano-spherical pitchblende distributed along the edges of Albite grains; (**C**) Pitchblende developed along the internal fissures of titanium oxides; (**D**) Film-like pitchblende occurring along the edges of micro-nano titanium oxide particles; (**E**,**F**) Dense symbiotic aggregates formed by pitchblende and titanium oxides. Q: Quartz; Ab: Ablite; Dol: Dolomite; U: Pitchblende; Ti: Ti-oxides; U-Ti: Pitchblende and Ti-oxides aggregates.

Uranium occurring in isomorphism is mainly hosted in Ti-oxides and dolomite (Figure 5). Uranium content in Ti-oxides varies between 0 wt% and 9.2 wt%. Uranium content in clay varies between 0% and 0.68%, while in dolomite it varies between 0% and 0.09% (Tables S2–S4).

Table 3. EPMA results of pitchblende in ore samples (wt%).

	CaO	UO_2	Y_2O_3	SiO_2	MgO	TiO_2	FeO	La_2O_3	Ce_2O_3	ZrO_2	P_2O_5	SO_3	PbO	Al_2O_3	Na_2O	Total
1	2.82	52.07	0.12	6.83	0.27	1.13	0.83	0.00	0.21	0.10	0.64	0.10	0.69	4.20	0.66	70.67
2	3.67	64.27	0.05	9.11	0.03	3.56	0.45	0.00	0.46	0.05	0.83	0.07	0.81	2.84	2.17	88.37
3	3.11	68.49	0.03	3.50	0.05	4.53	0.43	0.00	0.00	0.04	0.35	0.08	0.70	0.28	0.53	82.12
4	2.70	53.49	0.02	6.14	0.74	3.81	0.92	0.11	0.16	0.15	0.28	0.09	0.74	3.94	0.96	74.25
5	3.08	79.91	0.00	1.81	0.24	1.23	0.56	0.25	0.44	0.13	0.65	0.06	0.35	0.32	1.45	90.48
6	3.85	79.76	0.00	2.34	0.00	1.08	0.47	0.00	0.03	0.04	0.40	0.05	0.00	0.37	0.60	88.99
7	3.85	80.28	0.00	4.15	0.09	0.74	0.46	0.00	0.00	0.00	0.32	0.00	0.10	1.19	0.46	91.64
8	3.59	72.32	0.22	2.64	0.00	2.88	0.70	0.00	0.13	1.29	0.36	0.05	0.08	0.36	0.36	84.98
9	3.46	78.93	0.14	1.02	0.00	1.90	0.34	0.00	0.00	0.10	0.34	0.15	0.21	0.17	0.45	87.21
10	3.52	72.01	0.00	2.97	0.01	3.50	0.38	0.00	0.41	0.00	0.32	0.02	0.16	0.71	0.44	84.45
11	3.07	69.58	0.00	0.91	0.00	4.34	0.15	0.07	0.00	0.00	0.34	0.01	0.10	0.09	0.61	79.27
12	3.84	82.15	0.00	2.09	0.00	3.08	0.14	0.00	0.22	0.18	0.27	0.10	0.04	0.68	0.42	93.21
13	3.81	67.95	0.03	2.38	0.45	3.26	0.84	0.00	0.25	0.13	0.36	0.03	0.09	0.31	0.35	80.24
14	3.29	79.85	0.00	1.46	0.00	2.38	0.23	0.28	0.06	0.27	0.38	0.10	0.04	0.13	0.51	88.98
15	5.10	73.94	0.08	2.09	0.00	3.07	0.46	0.14	0.22	0.17	1.37	0.16	0.17	0.39	0.56	87.92
16	3.57	70.7.0	0.02	5.82	0.12	2.14	0.39	0.00	0.29	0.12	0.36	0.05	0.00	0.75	0.34	84.67
17	4.6	73.83	0.00	3.19	0.4	2.54	1.50	0.25	0.22	0.00	0.67	0.03	0.11	0.65	0.32	88.31
18	4.78	81.63	0.09	0.93	0.01	0.38	0.24	0.07	0.00	0.09	0.92	0.07	0.08	0.16	0.31	89.76
19	4.64	73.16	0.00	11.50	0.33	0.04	0.56	0.19	0.00	0.00	0.58	0.05	0.06	2.01	0.49	93.61
20	4.77	78.93	0.06	2.17	0.06	1.38	0.37	0.00	0.00	0.02	0.81	0.02	0.12	0.59	0.42	89.72
21	4.53	51.89	0.00	6.76	0.00	0.00	0.16	0.33	0.03	0.00	0.80	0.04	0.21	1.48	0.90	67.13
22	4.42	71.25	0.04	0.71	0.03	3.64	0.33	0.00	0.06	0.00	0.80	0.03	0.10	0.16	0.50	82.07
23	4.74	80.02	0.02	1.25	0.01	0.67	0.54	0.07	0.22	0.12	0.91	0.02	0.13	0.11	0.32	89.15
24	3.63	63.46	0.05	9.49	0.12	0.00	0.09	0.00	0.23	0.00	0.64	0.05	1.75	2.96	1.53	84.00
25	4.40	70.94	0.04	2.09	0.04	0.00	0.24	0.00	0.00	0.05	0.66	0.02	1.85	0.68	0.69	81.7
26	3.12	57.41	0.00	11.57	0.04	0.06	0.27	0.23	0.40	0.04	0.54	0.01	1.49	5.21	1.89	82.28
27	3.78	58.28	0.04	12.73	0.02	0.00	0.17	0.00	0.00	0.00	0.68	0.01	1.48	4.05	1.83	83.07
28	4.64	71.29	0.07	2.40	0.22	1.94	0.48	0.00	0.19	0.08	0.88	0.01	1.80	0.54	0.27	84.81
29	4.02	79.97	0.05	0.98	0.03	0.50	0.28	0.00	0.22	0.00	0.73	0.01	2.16	0.07	0.41	89.43
30	4.18	79.15	0.00	1.78	0.14	1.62	0.47	0.00	0.09	0.00	0.55	0.02	0.29	0.28	0.27	88.84
31	4.45	68.64	0.02	1.21	0.03	3.83	0.22	0.00	0.66	0.02	0.87	0.08	0.41	0.28	0.4	81.12
32	4.28	76.94	0.05	1.22	0.00	3.28	0.32	0.0	0.00	0.13	0.47	0.02	0.52	0.08	0.30	87.61
33	0.00	77.34	0.00	3.72	0.20	2.57	0.43	0.00	0.28	0.10	0.40	0.00	0.21	1.25	0.58	87.08
34	3.34	64.82	0.00	2.50	0.11	4.85	0.71	0.22	0.19	0.10	0.33	0.04	0.55	3.16	0.35	81.27
35	3.47	71.06	0.00	1.44	0.02	3.22	0.39	0.61	0.03	0.30	0.46	0.10	0.52	1.21	0.43	83.26
36	3.21	64.6	0.00	5.13	0.13	4.16	0.41	0.25	0.35	0.13	0.45	0.04	0.53	0.91	1.06	81.36
37	3.54	69.37	0.00	1.01	0.08	3.05	0.33	0.32	0.28	0.11	0.37	0.12	0.48	0.32	0.48	79.86
38	3.48	74.54	0.02	1.32	0.08	4.82	0.57	0.42	0.22	0.09	0.42	0.00	0.57	0.28	0.50	87.33
39	3.75	66.56	0.02	1.15	0.11	3.57	0.43	0.14	0.13	0.14	0.43	0.14	0.49	0.48	0.34	77.88
40	3.69	72.95	0.07	0.99	0.08	3.18	0.51	0.00	0.16	0.17	0.73	0.11	0.84	0.27	0.87	84.62
41	3.82	79.82	0.08	0.79	0.10	2.04	0.14	0.14	0.43	0.17	0.73	0.12	0.92	0.08	0.84	90.22
42	3.83	81.06	0.06	0.76	0.10	2.22	0.51	0.18	0.03	0.16	0.65	0.07	0.85	0.07	0.54	91.09
43	3.58	73.93	0.02	0.64	0.09	5.38	0.56	0.00	0.37	0.06	0.71	0.12	0.65	0.08	0.46	86.65

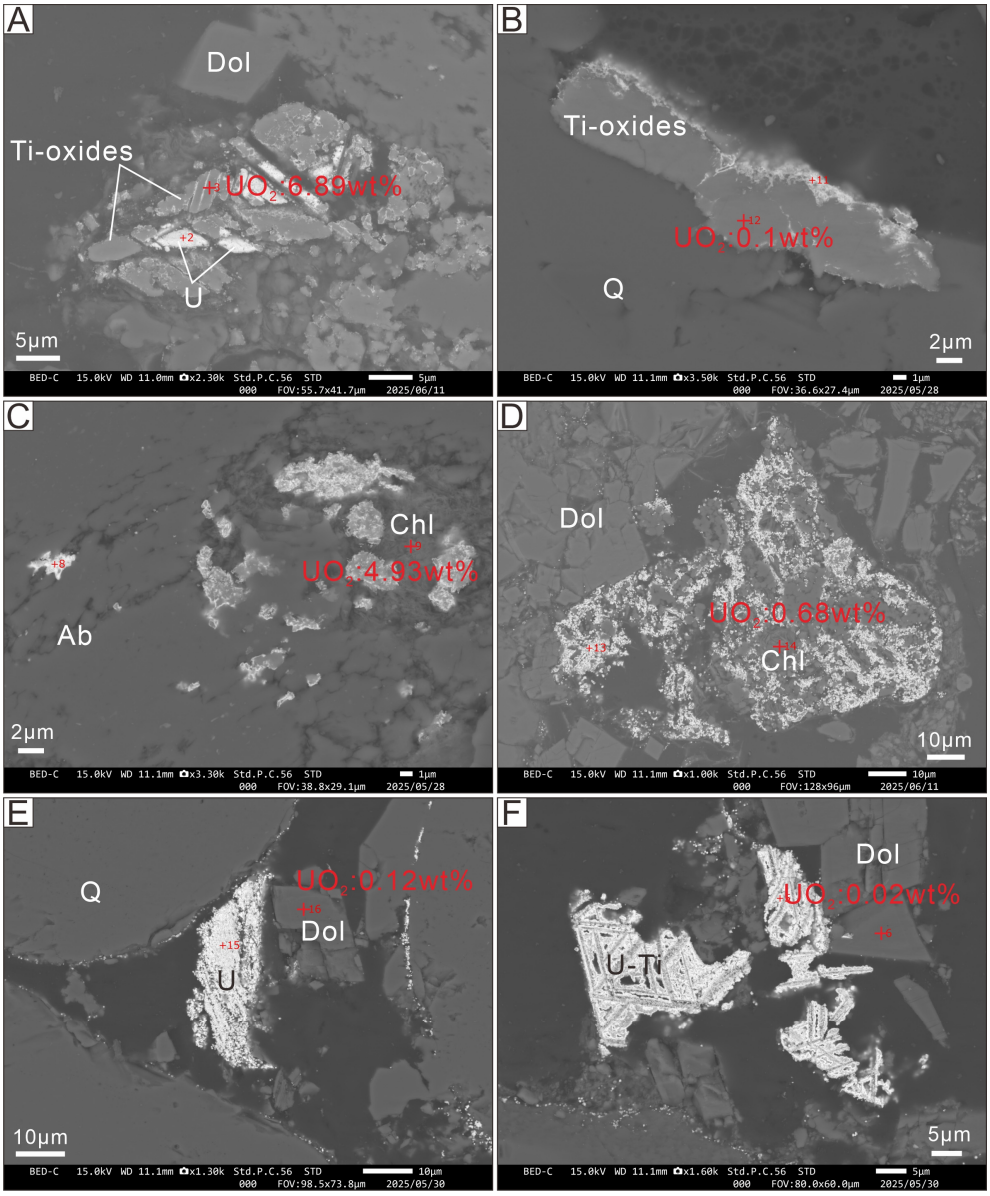

Figure 5. (**A**,**B**) Uranium hosted in titanium oxide crystals; (**C**,**D**) Uranium associated with clay minerals; (**E**,**F**) Uranium occurring in dolomite. The number with plus sign indicates the location of EPMA analysis. Dol: Dolomite; Q: Quartz; Ab: Albite; Chl: Chlorite.

4.5. Leaching Experiments

Thin-section leaching test: SEM observations revealed that nano-spherical pitchblende, film-like pitchblende distributed along Ti-oxides edges, and pitchblende forming aggregates with Ti-oxides all underwent significant dissolution, with most pitchblende dissolved and disappeared (Figure 6). Uranium-bearing Ti-oxides particles also exhibited partial dissolution (Figure 6B). Quartz and feldspar showed no observable dissolution features (Figure 6). Both euhedral and anhedral dolomite particles underwent partial dissolution during leaching, forming dissolution pits on mineral surfaces (Figure 7). Pyrite also showed slight dissolution, with surfaces becoming rougher after leaching compared to before (Figure 7).

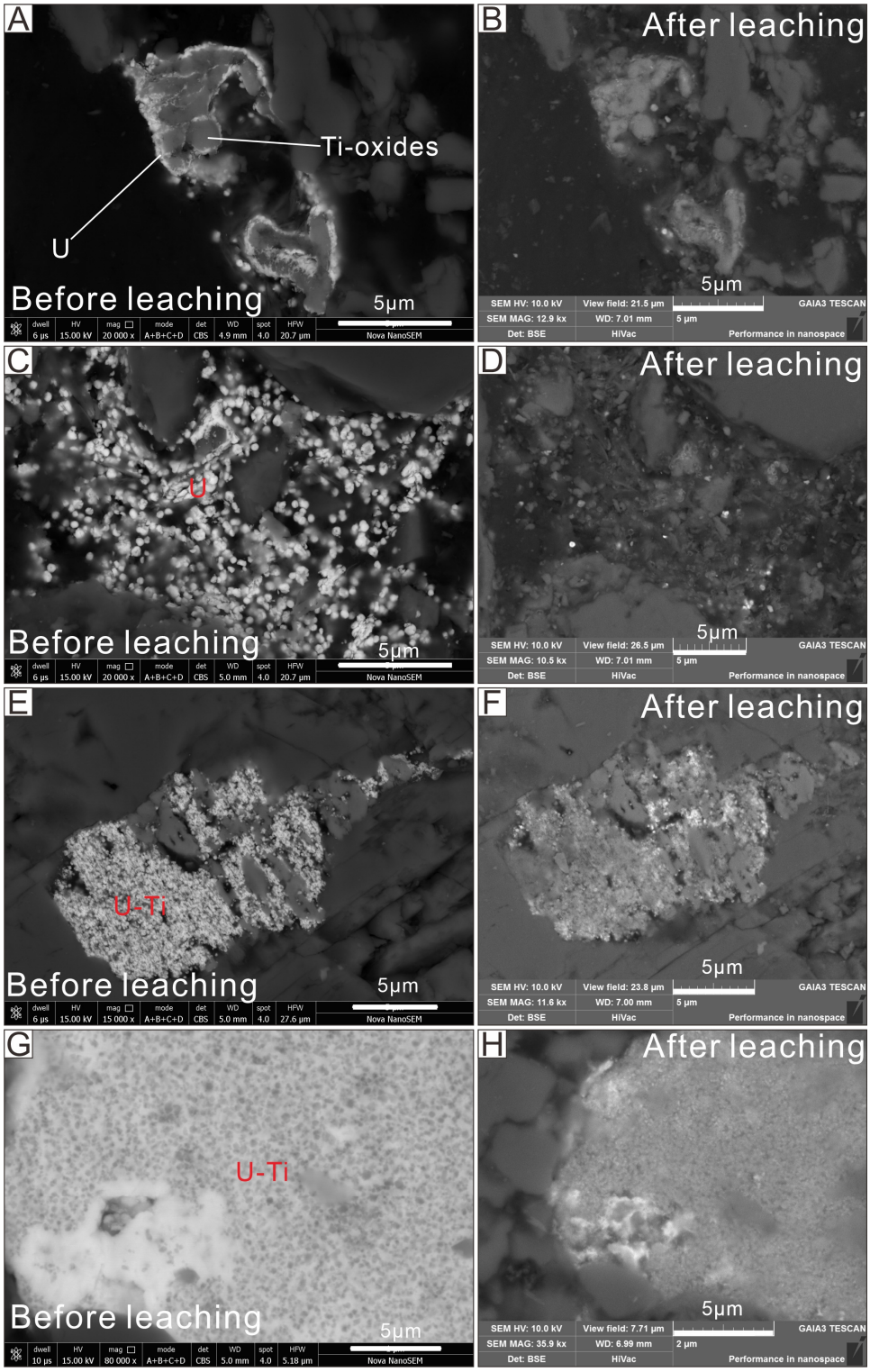

Figure 6. The morphology of pitchblende before and after leaching under CO_2 + O_2 condition. (**A**,**B**) Film-like pitchblende completely dissolved and disappeared after leaching, while uranium-bearing titanium oxides exhibited slight corrosion, showing reduced particle size and curved edges; (**C**,**D**) Nano-spherical pitchblende fully dissolved after leaching; (**E**–**H**) Pitchblende closely symbiotic with titanium oxides completely dissolved, leaving behind residual titanium oxides.

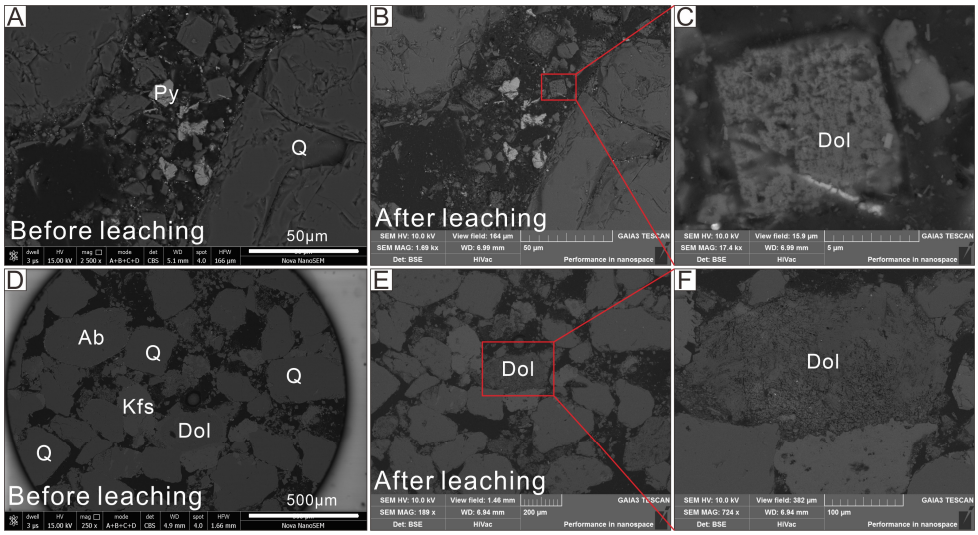

Figure 7. The morphology of dolomite and pyrite before and after leaching under CO_2 + O_2 condition. (**A**–**C**) The dissolution pits and cavities were developed in euhedral dolomite grains after CO_2 + O_2 leaching. The surface of pyrite grains becomes rougher. (**D**–**F**) Quartz, plagioclase and K-feldspar grains show no evidence of dissolution, dissolution occur in dolomite grains.

For stirred leaching experiments, powder samples were derived from ores of different drill holes. These ores were crushed to their natural grain size and mixed. The major elements in the ore were quantitatively analyzed using XRF (Table 4), and uranium content was determined by chemical titration, yielding a value of 0.031%.

Table 4. XRF results of experimental samples before leaching (wt%).

SiO_2	CaO	Al_2O_3	MgO	K_2O	Na_2O	Fe_2O_3	TiO_2	P_2O_5
78.700	6.900	6.170	3.200	1.970	1.460	0.886	0.200	0.178
SO_3	WO_3	U	MnO	Cl	SrO	Rb_2O	ZrO_2	ZnO
0.152	0.028	0.027	0.026	0.026	0.011	0.006	0.006	0.003

Acid Stirring Leaching: The leaching results show that as acid concentration increased from 5 g/L to 25 g/L, pH continuously decreased. Uranium concentration in the leachate increased from 9 mg/L to 56 mg/L, accompanied by an increase in leaching recovery from 14.52 wt% to 90.32 wt%. However, acid consumption per ton of ore also increased from 25 kg/t to 79.2 kg/t. Residual acid only appeared in the solution when sulfuric acid concentration exceeded 15 g/L, after which the rate of increase in acid consumption slowed significantly (Table 5).

Table 5. Sulfuric acid Stirring leaching results.

H_2SO_4 (g/L)	pH	Eh (mv)	U (mg/L)	Residual Acid (g/L)	Acid Consumption of Ore (kg/t)	Leaching Rate (wt%)
5	5.89	103	9	0.00	25.0	14.52
10	5.24	121	6	0.00	50.0	8.06
15	2.49	291	45	0.00	75.0	72.58
20	1.26	357	56	4.17	79.2	90.32

Alkaline Stirring Leaching: Results showed that as NH_4HCO_3 concentration increased from 1.5 g/L to 3.0 g/L, uranium concentration increased from 30 mg/L to 38.0 mg/L, and leaching recovery increased from 48.39% to 61.29%. Using a 3 mg/L NH_4HCO_3 solution with additions of 0.1 g/L and 0.2 g/L $KMnO_4$ showed that leaching recovery increased

substantially with oxidant addition, exceeding 90%, indicating oxidizers effectively promote uranium leaching (Table 6).

Table 6. Alkaline Stirring Leaching results.

NH_4HCO_3 (g/L)	U (mg/L)	pH	Eh (mV)	Leaching Rate (wt%)
1.5	30.0	8.33	131	48.39
2.0	34.0	8.29	129	54.84
2.5	37.0	8.22	160	59.68
3.0	38.0	8.23	155	61.29

CO_2 + O_2 Pressurized Stirring Leaching: Results showed that under an 8-day leaching cycle, as O_2 pressure increased from 1 MPa to 2 MPa, leaching recovery increased from 70.97% to 82.26%. Under 1 MPa O_2, as leaching duration increased from 5 days to 10 days, recovery increased from 69.35% to 74.19% (Table 7).

Table 7. CO_2 + O_2 Pressurized Stirring Leaching results.

O_2 Pressure (MPa)	U (mg/L)	pH	Eh (mV)	Leaching Rate (wt%)
1.0	44.0	7.22	197	70.97
1.5	45.0	7.14	203	72.58
2.0	51.0	7.83	188	82.26

CO_2 + O_2 Pressurized Column Leaching Test: The results showed that final liquid (mL)-to-solid (mg) (L/S) ratio reached 5.18, and the cumulative leaching recovery was 68.45%. A peak uranium concentration of 158 mg/L was observed during the leaching, with an average concentration of 36.4 mg/L in the leachate. Compared to the results from previous CO_2 + O_2 pressurized column leaching tests on different ore samples, the outcome of this test was considered favorable.

During the leaching process, when the L/S ratio reached approximately 3.20, a continuous decline in both uranium and bicarbonate (HCO_3^-) concentrations in the leachate was observed. To address this, the leaching agent preparation tank was depressurized, and fresh CO_2 was injected at an increased pressure of 0.3 MPa to replenish the carbonate source. After 24 h of CO_2 addition, O_2 was introduced under pressure at 1.0 MPa. Subsequently, when the L/S ratio reached about 3.49, the O_2 pressure was further increased to 1.3 MPa. Shortly after these adjustments in CO_2 and O_2 pressures, a minor peak of slightly elevated uranium concentration appeared in the leachate. Following this small peak, the uranium concentration continued to decrease until the end of the leaching experiment.

5. Discussion

The uranium occurrence state, the types and abundance of gangue minerals, and the pore structure of the ore are critical factors influencing the ISR efficiency of sandstone-hosted uranium deposits [2]. The combined observations and analyses by SEM-EDS and EPMA confirm that uranium in the Zhenyuan Deposit primarily exists as pitchblende (Figure 4). Additionally, a small fraction occurs as solid solution within Ti-oxides and dolomite lattices, while a trace amount is adsorbed onto chlorite (Figure 5, Tables 3 and S2–S4).

Pitchblende (uraninite) is the most economically significant uranium mineral globally. Compared to other economically important uranium minerals like coffinite and brannerite, pitchblende is more amenable to leaching [8]. The dissolution of pitchblende under CO_2 + O_2 leaching condition involves: (1) The oxidation of tetravalent uranium (U^{4+}) to hexavalent uranium (U^{6+}) on the surface; (2) binding of HCO_3^{2-} at the U(VI) sites of the oxidized layer; and (3) detachment of the U(VI)-carbonato surface complex [21,22].

In the CO_2 + O_2 leaching system, oxygen (O_2) acts as the primary oxidant. Meanwhile, dissolved CO_2 forms carbonic acid (H_2CO_3), which dissociates to provide bicarbonate ions (HCO_3^-). Additionally, the reaction between H_2CO_3 and carbonate minerals such as calcite and dolomite, produce HCO_3^-, which then serves as a complexing ligand for uranyl ions (UO_2^{2+}). The oxidation of U^{4+} under weakly acidic to near-neutral conditions is a pseudo-first-order reaction. The oxidation mechanism involves the adsorption of oxygen onto the pitchblende surface, the formation of pentavalent uranium (U^{5+}), and its subsequent reaction with oxygen. Once sufficient U^{6+} accumulates, its reaction with remaining U^{4+} to form U^{5+} may become the rate-limiting step [8,12]. Ultimately, U^{6+} reacts with bicarbonate to form soluble uranyl carbonate complexes, predominantly uranyl tricarbonate $[UO_2(CO_3)_3]^{4-}$ [6]. The thin-section leaching results demonstrate that pitchblende particles were completely dissolved under the experimental conditions of 0.2 MPa CO_2 for 4 h followed by 1 MPa O_2 for 7 days (Figure 6). This confirms the high leachability of pitchblende in this deposit. Moreover, both stirred tank and column leaching experiments yielded high uranium recovery rates, substantiating the effectiveness of the CO_2 + O_2 method for Zhenyuan ores. Importantly, SEM observations reveal that pitchblende in the Zhenyuan Deposit predominantly occurs as nano-spherical particles and as thin films (<2 μm thick) coating the surfaces of Ti-oxides. Such morphologies substantially increase the specific surface area of the uranium-bearing phases, maximizing the contact area with the lixiviant and thus favoring rapid dissolution (Figure 4). Furthermore, pitchblende was not found to be encapsulated by either refractory silicate minerals (e.g., quartz, feldspar) or readily soluble carbonates (e.g., calcite), indicating a high degree of mineral liberation. A high liberation degree is also conducive to efficient contact and reaction between uranium minerals and the leaching reagents. In addition to pitchblende, uranium also exists within Ti-oxide and dolomite lattices. The SEM observations from thin-section leaching experiments confirmed that both Ti-oxide and dolomite underwent partial dissolution to varying degrees. Therefore, this portion of uranium can also be extracted during the leaching process. In summary, the favorable uranium occurrence characteristics in Zhenyuan ores—primarily as accessible pitchblende with high specific surface area and liberation degree—are all advantageous for uranium extraction.

The types and abundances of gangue minerals also significantly influence uranium leaching. In Zhenyuan ores, quartz and feldspar account for an average of approximately 93.6 wt%, with quartz content typically exceeding 85 wt%. These framework silicate minerals are chemically stable under leaching conditions and react minimally with lixiviants, which is beneficial for the process. However, the ores also contain more than 5 wt% of dolomite and calcite. These carbonates are primarily distributed along the edges of quartz-feldspar framework grains, creating more complex and variable pore structures. Such complexity can increase turbulence and hydraulic resistance during the injection-production cycle, leading to higher injection pressures. Our analysis further indicates that in samples with comparable porosity, the presence of dolomite significantly reduces both gas and liquid permeability, suggesting a damaging effect on rock permeability. Under sulfuric acid leaching conditions, dolomite would react vigorously, resulting in unacceptably high acid consumption and increased economic costs for deposit exploitation. Moreover, this reaction promotes gypsum ($CaSO_4 \cdot 2H_2O$) precipitation, potentially clogging the ore-bearing aquifer. Given the high carbonate mineral content in this deposit and the high acid consumption confirmed by stirred leaching tests, the sulfuric acid leaching method is not suitable for the Zhenyuan Deposit. In contrast, under CO_2 + O_2 leaching conditions, calcite dissolves completely, and dolomite undergoes significant partial dissolution (Figure 7). The dissolution of carbonate minerals enhances the bicarbonate concentration in the groundwater, providing essential ligands for uranium complexation and thus fa-

cilitating uranium extraction. The column leaching test results showed that when the L/S ratio reached approximately 3.2, the bicarbonate concentration in the leachate began to decrease, accompanied by a synchronous decline in uranium concentration (Table 8). This likely indicates that the inherent carbonate minerals in the ore were insufficient to supply the HCO_3^- required for sustained leaching. Notably, increasing the CO_2 pressure subsequently led to a temporary increase in uranium concentration, highlighting the role of carbonate dissolution. In a practical ISR operation, where ore-bearing aquifer water is continuously recirculated between injection and production wells, bicarbonate ions would accumulate over time, further promoting leaching. Furthermore, porosity and permeability tests indicate that the Zhenyuan Deposit possesses relatively high porosity and permeability (Table 2). Both XRD and SEM results show that the clay mineral content in the ore is very low (Table 1 and Figure 1). The intergranular pore spaces are primarily filled with dolomite and calcite, or these minerals line the framework grain boundaries (Figure 1). Therefore, the dissolution of these carbonates during CO_2 + O_2 leaching can also improve the overall permeability of the deposit [23]. Additionally, the well-consolidated nature of the ore, coupled with low contents of clay and fine-grained quartz/feldspar particles within the pores, will help minimize particles migration during leaching. This reduces the risk of aquifer clogging and the associated decline in injection and production rates often encountered during ISR operations due to particle clogging. While the thin-section leaching confirmed that the dissolution of dolomite was limited at 0.2 MPa CO_2, it also demonstrated that its dissolution not only contributes to bicarbonate ions but also enhances permeability. Thus, we recommend employing higher CO_2 injection pressure during actual mining operations.

The Zhenyuan ores also contain minor pyrite. Pyrite is considered a significant oxygen-consuming mineral during CO_2 + O_2 leaching. Furthermore, its oxidation produces sulfate ions, which can combine with calcium ions to form gypsum precipitates, while ferric iron (Fe^{3+}) forms iron hydroxide colloids, both potentially clogging the ore-bearing aquifer. However, the thin-section leaching results suggest that the degree of pyrite dissolution under 0.2 MPa CO_2 + 1 MPa O_2 was far less pronounced compared to pitchblende and dolomite (Figure 7). Therefore, in the initial leaching stages, pyrite may not be the primary oxygen consumer. Due to its relatively slow dissolution rate, the negative impact of its oxidation products (e.g., gypsum, $Fe(OH)_3$) on permeability may also be limited initially. Nonetheless, as leaching progresses with continued pyrite dissolution, the permeability damage from these precipitates could increase over time.

Overall, the key characteristics of the Zhenyuan Deposit—high content of stable framework silicates (quartz, feldspar), well-consolidated rock fabric, significant but manageable carbonate mineral content, low sulfide (e.g., pyrite) abundance, and uranium primarily occurring in highly leachable pitchblende forms—collectively indicate excellent leachability. These features strongly suggest that the deposit is well-suited for exploitation using the CO_2 + O_2 ISR process. Additionally, we recommend that appropriately increasing the CO_2 injection pressure during operation to enhance dolomite dissolution would further optimize leaching efficiency.

Table 8. The results of CO_2 + O_2 Pressurized Column Leaching Test.

Leachate Volume (mL)	Total Volume (mL)	U (g/L)	U (g)	Leaching Rate (wt%)	Liquid-Solid Ratio	pH	Eh (mV)
315	315	0.1580	0.04977	30.68	0.45	8.54	170
65	380	0.0880	0.00572	33.31	0.54	8.60	170
60	440	0.1240	0.00744	36.74	0.63	8.36	184
90	530	0.1230	0.01107	41.84	0.76	8.36	197
74	604	0.0820	0.00607	44.64	0.86	8.44	200
64	668	0.0570	0.00365	46.32	0.95	8.15	209
65	733	0.0520	0.00338	47.89	1.05	8.22	213
76	809	0.0460	0.00350	49.49	1.16	8.21	214
94	903	0.0370	0.00348	51.09	1.29	8.31	216
58	961	0.0330	0.00190	51.97	1.37	8.37	216
82	1043	0.0330	0.00271	53.22	1.49	8.18	221
90	1133	0.0280	0.00252	54.38	1.62	8.10	222
88	1221	0.0250	0.00220	55.40	1.74	8.08	227
89	1310	0.0210	0.00187	56.26	1.87	8.08	234
104	1414	0.0170	0.00177	57.07	2.02	7.88	239
93	1507	0.0170	0.00158	57.80	2.15	7.95	239
95	1602	0.0150	0.00143	58.46	2.29	7.90	242
86	1688	0.0140	0.00120	59.01	2.41	7.86	243
76	1764	0.0140	0.00106	59.50	2.52	7.85	247
77	1841	0.0130	0.00100	59.96	2.63		
65	1906	0.0140	0.00091	60.38	2.72		
120	2026	0.0150	0.00180	61.21	2.89	8.13	200
123	2149	0.0150	0.00185	62.06	3.07	8.10	204
90	2239	0.0150	0.00135	62.69	3.20	7.58	194
103	2342	0.0150	0.00155	63.40	3.35		
39	2381	0.0160	0.00062	63.68	3.40		
30	2411	0.0170	0.00051	63.92	3.44		
31	2442	0.0170	0.00053	64.16	3.49	8.22	207
30	2472	0.0170	0.00051	64.40	3.53	8.00	209
55	2527	0.0190	0.00105	64.88	3.61	7.79	214
55	2582	0.0170	0.00094	65.31	3.69	7.68	217
39	2621	0.0150	0.00059	65.58	3.74	8.26	350
107	2728	0.0120	0.00128	66.17	3.90	8.50	351
80	2808	0.0100	0.00080	66.54	4.01	8.53	345
150	2958	0.0080	0.00120	67.09	4.23	8.56	336
130	3088	0.0070	0.00091	67.51	4.41	8.50	334
110	3198	0.0060	0.00066	67.82	4.57	8.50	331
130	3328	0.0050	0.00065	68.12	4.75	8.31	334
115	3443	0.0020	0.00026	68.24	4.92	8.06	341
180	3623	0.0026	0.00047	68.45	5.18	7.61	361

6. Conclusions

(1) Uranium in the Zhenyuan Deposit predominantly exists as nano-spherical and film-like pitchblende. A minor portion occurs as solid solution within the crystal lattices of Ti-oxides and dolomite, while a trace amount is adsorbed onto clay minerals.

(2) Under CO_2 + O_2 leaching conditions, pitchblende is effectively and completely dissolved. Dolomite undergoes significant partial dissolution, while pyrite exhibits the least dissolution among the studied minerals.

(3) The Zhenyuan Sandstone Uranium Deposit is well-suited for exploitation using the CO_2 + O_2 in situ leaching process. Furthermore, to optimize the process, it is advisable to increase the CO_2 injection pressure appropriately during operation to promote more extensive dolomite dissolution, thereby enhancing bicarbonate availability and ore permeability.

Supplementary Materials: The following supporting information can be downloaded at: https://www.mdpi.com/article/10.3390/min16040340/s1, Table S1: Porosity, gas permeability and liquid permeability of ore sample; Table S2: EPMA results of Ti-oxides; Table S3: EPMA results of clay; Table S4: EPMA results of dolomite.

Author Contributions: Conceptualization, C.H.; methodology, C.H.; investigation, C.H., S.C., Y.Z. (Ying Zhang), Z.L., X.X., J.D., Y.Z. (Yuhan Zou) and W.L.; data curation, J.D. and Y.Z. (Yuhan Zou); writing—original draft preparation, C.H.; writing—review and editing, C.H.; funding acquisition, C.H. and W.L. All authors have read and agreed to the published version of the manuscript.

Funding: This research was funded by China National Nuclear Corporation (Grant No. CNNC-JCYJ-202689 and CNNC-JCYJ-202332) and National Key Laboratory of Uranium Resources Exploration-Mining and Nuclear Remote Sensing (Grant No. NKLUR-WDZC-2025-05 and NKLUR-WDZC-2024-HHYY-03).

Data Availability Statement: The data in this article has been submitted to MDPI.

Acknowledgments: We would like to thank three anonymous reviewers for their constructive reviews. We also thank Liumin Deng at Beijing Research Institute of Uranium Geology for support during SEM, EPMA and XRD analysis.

Conflicts of Interest: Authors Chunru Hou, Zhengbang Liu, Jinxun Deng, Yuhan Zou and Wensheng Liao were employed by the company CNNC. Authors Shihai Chen and Ying Zhang were employed by the PetroChina Changqing Oilfield Company. Author Xiansheng Xie was employed by the company China Shaanxi Nuclear Industry Group Geological Survey Institute Co., Ltd. All authors declare that the research was conducted in the absence of any commercial or financial relationships that could be construed as a potential conflict of interest.

Abbreviations

The following abbreviations are used in this manuscript:

ISR	In situ recovery
Q	Quartz
Ab	Albite
Kfs	K-feldspar
U	Pitchblende
Ti	Ti-oxide
Chl	chlorite

References

1. Li, G.; Yao, J. A Review of In Situ Leaching (ISL) for Uranium Mining. *Mining* **2024**, *4*, 120–148. [CrossRef]
2. Qiao, P.; Xiong, Q.; Ge, L.; Song, H.; Yu, H.; Yang, Y.; Wang, R.; Kang, S.; Zhou, Y.; Fan, Y. The influence of mineralogical characteristics and pH on uranium extraction via in-situ leaching: Preliminary case analysis of the Hadatu uranium deposit, China. *Hydrometallurgy* **2025**, *235*, 106492. [CrossRef]
3. Ram, R.; Charalambous, F.A.; Mcmaster, S.; Pownceby, M.I.; Tardio, J.; Bhargava, S.K. Chemical and micro-structural characterisation studies on natural uraninite and associated gangue minerals. *Miner. Eng.* **2013**, *45*, 159–169. [CrossRef]
4. Wang, B.; Luo, Y.; Li, X.; Liu, Y.Z.; Xu, C.R.; Zheng, Y.X.; Zhang, Y.H.; Zhou, Y.R. Water–Rock reactions in the acid leaching of Uranium: Hydrochemical characteristics and reaction mechanisms. *J. Hydrol.* **2024**, *641*, 131798. [CrossRef]
5. Wang, P.; Tan, K.; Li, Y.; Liu, Z.; Li, C.; Tan, W.; Tian, Y.; Huang, W. Effect of Pyrite on the Leaching Kinetics of Pitchblende in the Process of Acid In Situ Leaching of Uranium. *Minerals* **2022**, *12*, 570. [CrossRef]
6. Weng, H.; Yuan, Y.; Liu, Z.; Hou, C. Simulation study on mineral dissolution and precipitation during the "CO_2+O_2" in-situ leaching process. *Uranium Min. Metall.* **2025**, *4*, 19–84.
7. Youlton, B.J.; Kinnaird, J.A. Gangue–reagent interactions during acid leaching of uranium. *Miner. Eng.* **2013**, *52*, 62–73. [CrossRef]
8. Shilov, V.P.; Yusov, A.B.; Peretrukhin, V.F.; Delegard, C.H.; Gogolev, A.V. Oxidation of U(IV) by atmospheric oxygen in pH 1.5–7.4 aqueous solutions. *J. Alloys Compd.* **2007**, *444*, 333–338. [CrossRef]
9. Casas, I.; de Pablo, J.; Gimenez, J.; Torrero, M.E.; Bruno, J.; Cera, E.; Finch, R.J.; Ewing, R.C. The role of pe, pH, and carbonate on the solubility of UO_2 and uraninite under nominally reducing conditions. *Geochim. Cosmochim. Acta* **1998**, *62*, 2223–2232. [CrossRef]
10. De Pablo, J.; Casas, I.; Giménez, J.; Molera, M.; Rovira, M.; Duro, L.; Bruno, J. The oxidative dissolution mechanism of uranium dioxide. i. The effect of temperature in hydrogen carbonate medium. *Geochim. Cosmochim. Acta* **1999**, *63*, 3097–3103. [CrossRef]
11. Torrero, M.E.; Baraj, E.; Pablo, J.D.; Giménez, J.; Casas, I. Kinetics of corrosion and dissolution of uranium dioxide as a function of ph. *Int. J. Chem. Kinet.* **1997**, *29*, 261–267. [CrossRef]

12. Eary, L.E.; Cathles, L.M. A Kinetic Model of UO_2 Dissolution in Acid, H_2O_2 Solutions That Includes Uranium Peroxide Hydrate Precipitation. *Metall. Trans. B* **1982**, *14*, 325–334. [CrossRef]
13. Qiu, W.; Yang, Y.; Song, J.; Que, W.; Liu, Z.; Weng, H.; Wu, J.; Wu, J. What chemical reaction dominates the CO_2 and O_2 in-situ uranium leaching? Insights from a three-dimensional multicomponent reactive transport model at the field scale. *Appl. Geochem.* **2022**, *148*, 105522. [CrossRef]
14. Avasarala, S.; Torres, C.; Ali, A.M.S.; Thomson, B.M.; Spilde, M.N.; Peterson, E.J.; Artyushkova, K.; Dobrica, E.; Lezama-Pacheco, J.S.; Cerrato, J.M. Effect of bicarbonate and oxidizing conditions on U(IV) and U(VI) reactivity in mineralized deposits of New Mexico. *Chem. Geol.* **2019**, *524*, 345–355. [CrossRef] [PubMed]
15. Vogt, T.C.; Strom, E.T.; Johnson, W.F.; Venuto, P.B. In-situ leaching of Crownpoint, NM, uranium ore. iii. laboratory study of strong leaching systems: Sodium hypochlorite. *Soc. Pet. Eng. J.* **1985**, *25*, 875–880. [CrossRef]
16. Hu, M.; Niu, Q.; Yuan, W.; Wang, W.; Chang, J.; Du, Z.; Wang, Q.; Zheng, Y.; Shangguan, S.; Qi, X.; et al. Evolution characteristic and mechanism of microstructure, hydraulic and mechanical behaviors of sandstone treated by acid-rock reaction: Application of in-situ leaching of uranium deposits. *J. Hydrol.* **2024**, *643*, 131948. [CrossRef]
17. Zhang, T.; Sun, T.; Miao, A. *Preliminary Exploration Report on the Mengba Uranium Deposit, Zhenyuan County, Gansu Province, from Exploration Lines M5 to M49*; China National Nuclear Corporation (CNNC): Beijing, China, 2024.
18. Zhao, K.; Sun, Z.; Du, C.; Zhou, Y.; Li, G.; Lui, J.; Xu, L. Blockage and uranium migration via CO_2+O_2 leaching within autoclave: A test study from Mengqiguer deposit in Yili Basin, Northwest of China. *J. Radioanal. Nucl. Chem.* **2022**, *331*, 2631–2644. [CrossRef]
19. Fan, Y.; Song, H.; Wang, Z.; Gan, N.; Zhang, C.; Zhao, B.; Xu, Z.; Tan, Y. The behavior of pyrite during in-situ leaching of uranium by CO_2+ O_2: A case study of the Qianjiadian uranium deposit in the Songliao Basin, northeastern China. *Ore Geol. Rev.* **2024**, *169*, 106085. [CrossRef]
20. Luo, J.; Cui, G.; Yang, D.; Huo, C.; He, G.; Fu, H.; Yang, C. Impact of the existence of carbonate minerals on the performance of CO_2+O_2 during in situ leaching in uranium deposits. *Nucl. Eng. Technol.* **2025**, *57*, 103821. [CrossRef]
21. Niu, Q.; Wang, J.; He, J.; Yuan, W.; Chang, J.; Wang, W.; Yuan, J.; Wang, Q.; Zheng, Y.; Shang, S. Evolution of pore structure, fracture morphology and permeability during CO_2+O_2 in-situ leaching process of fractured sandstone. *Energy* **2025**, *315*, 134348. [CrossRef]
22. Reynolds, H.S.; Ram, R.; Pownceby, M.I.; Yang, Y.; Chen, M.; Tardio, J.; Jones, J.; Bhargava, S.K. Kinetics of uranium extraction from coffinite—A comparison with other common uranium minerals. *Trans. Nonferrous Met. Soc. China* **2018**, *28*, 2135–2142. [CrossRef]
23. Luquot, L.; Gouze, P. Experimental determination of porosity and permeability changes induced by injection of CO_2 into carbonate rocks. *Chem. Geol.* **2009**, *265*, 148–159. [CrossRef]